Transport properties of functionally graded materials

Moran Wang[a)]
Nanomaterials in the Environment, Agriculture and Technology, University of California at Davis, California 95616

Fankong Meng
School of Aerospace, Tsinghua University, Beijing 100084, China

Ning Pan
Nanomaterials in the Environment, Agriculture and Technology, University of California at Davis, California 95616

(Received 30 April 2007; accepted 25 June 2007; published online 10 August 2007)

This paper presents a numerical method to predict the effective transport properties of multiphase functionally graded materials, accounting for the effects of random phase distribution and multiphase interactions. Firstly, the multiphase microstructures of such graded materials are reproduced by a random generation-growth algorithm, and then the corresponding transport governing equations are solved using a high-efficiency lattice Boltzmann method. The predicted effective electric and thermal conductivities agree well with the existing experimental data for both two- and three-phase functionally graded materials. Furthermore when the methodology is extended to other transport and even nontransport physical properties of multiphase composites, our simulated results still agree much better with the available experimental data than the existing theoretical models. This may exhibit the robusticity and wider applicability of the present approach. © *2007 American Institute of Physics*. [DOI: 10.1063/1.2767629]

I. INTRODUCTION

Functionally graded materials (FGMs) are a class of materials with spatially varied microstructures of constituent phases and gradual variation of effective material properties tailored for specific performance requirements.[1,2] Such materials have recently gained more attention owing to their unique transport properties that are suited to special applications,[1–3] for instance, as advanced heat-shielding materials in aerospace and electronics industries.[4–6] FGM has also been used in actuator devices where the materials behave better than the bimorph actuators in thermal resistance, peeling resistance, and reliability due to the absence of bonding agents.[7,8] Another electrical application of FGM is as a heat-electricity conversion material for design of energy conversion systems, likely raising the conversion efficiency by above 40% from a nuclear or solar source.[9,10] Comprehensive reviews and analyses of FGM can be found in some recent books,[1,2,11] journals, and conference proceedings.[12–14]

Given the complexity and versatility, it becomes highly desirable to develop modeling and prediction tools for FGM behaviors in design and optimization for sophisticated applications. Some theoretical models and numerical methods have been established in the past decade.[1,8,11–21] However, most analytical models deal with two-phase cases only, very few are able to tackle the spatial variation in microstructure of FGMs,[16] and virtually none of them has addressed the issue of interactions between different phases.[17] As the computational technique advances, numerical simulations provide a more powerful way to investigate the effects of phase distribution and interactions in microstructures on the effective properties of FGMs. For instance, a few partial differential equation (PDE) solvers, such as finite difference method (FDM), finite element method (FEM), and boundary element method (BEM), have been employed to predict the effective conductivities of FGMs.[18–21] However, such conventional PDE solvers encountered two problems once the phase distributions in heterogeneous multiphase materials become complex. Firstly, the accuracy of these conventional numerical methods is strongly dependent on the grid size so that an extra fine grid is needed whenever the transport process gets complicated either in physics or in geometry. The requirement of grid refinement for complex phase distribution and interactions in FGMs often restrict the computational domain into a very limited area. The second is the conjugate constraint on interfaces between different phases: for steady transport through multiphase structures, the continuities of the potentials and fluxes have to be ensured at the interfaces when solving the governing equations, thus demanding enormously high computational resources for a FGM with numerous interfaces in the material. To overcome these two difficulties, the present authors have proposed a high-efficiency lattice Boltzmann algorithm[22,23] to solve the transport governing equations in multiphase systems, by which the conservation and continuity constraints are self-satisfied so that a much smaller grid number is required for the same accuracy comparing with other PDE solvers. Our method has been employed for predicting thermal properties of various microporous media and the results agree well with the existing experimental data.[24–26]

The objective of this contribution is to investigate the effective conductivities of multiphase FGMs by numerical simulations. With our method, the microstructures of given

[a)]Electronic mail: mmwang@ucdavis.edu

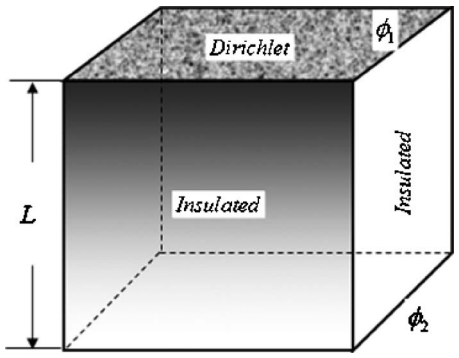

FIG. 1. Schematic diagram of domain and boundaries.

FGMs are generated in the computer by a random generation-growth method[24] accounting for the effects of multiphase distribution and interactions, and then the transport governing equations are solved by our high-efficiency lattice Boltzmann algorithm with necessary modifications. Also because of the similarities between the thermal and electric conduction physics, we group the two into one problem of dealing with the material conductivity. The calculated results will be compared with both the existing theoretical predictions and experimental data.

II. NUMERICAL METHODS

A. Governing equations

To determine the effective conductivity of a multiphase FGM as a cubic system ($L\times L\times L$) in Fig. 1, we assume no convection, no radiation, no heat source, and no phase change during the heat transfer in a steady pure heat conduction problem, or similarly in an electrical conduction problem; both the electric-magnetic effect and contact resistance at the interfaces between different phases are negligible. The top and bottom surfaces of the cube are Dirichlet boundaries and the other four surfaces are insulated.

Therefore, the transport governing equations through such a multiphase system are

$$\nabla\cdot(\lambda_n\nabla\phi)=0, \tag{1}$$

where λ_n is the conductivity of the nth phase, which could be the thermal conductivity (k) or the electric conductivity (σ) for a given case, and correspondingly, ϕ would be the thermal potential/temperature (T) or the electric potential (Φ).[27,28]

At the interfaces between two phases in equilibrium, the continuities of both potential and flux have to be satisfied, i.e.,

$$\phi_{\text{int},1}=\phi_{\text{int},2}, \tag{2}$$

$$\lambda_1\ \nabla\phi|_{\text{int},1}=\lambda_2\ \nabla\phi|_{\text{int},2}, \tag{3}$$

where the subscript "int" corresponds to the interfaces, "1" to phase 1 and "2" to phase 2. Equation (1) thus governs the distribution of potential ϕ in the multiphase FGM, subject to the interface constraints Eqs. (2) and (3). After the potential field is derived, the effective conductivity can be determined as

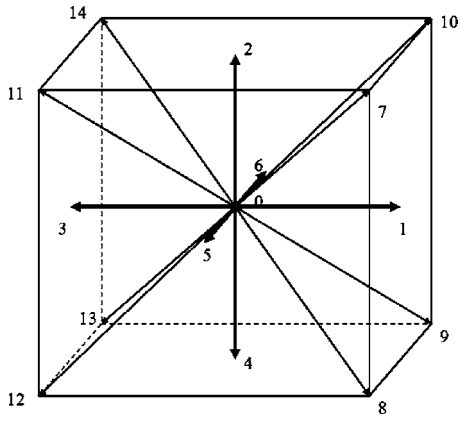

FIG. 2. The lattice direction system (α) for D3Q15 model.

$$\lambda_{\text{eff}}=qL/\Delta\phi, \tag{4}$$

where q is the steady flux through the material between the potential difference ($\Delta\phi$) over a thickness L.

As stated before, the complexity of phase distributions in FGMs and the continuity constraint at huge numbers of phase interfaces increase the computational costs tremendously when using the conventional PDE solvers to solve the governing equations. We thus have to adopt an alternative route.

B. The lattice Boltzmann model

The lattice Boltzmann method (LBM) is intrinsically a mesoscopic approach based on simulating the evolution of statistical distribution of particles on lattices, and has achieved considerable success in simulating fluid flows and associated transport phenomena.[29–31] The most important advantages of LBM are the natural incorporation of interparticle interactions and the easy implementation of complex geometry boundary conditions.[32–35] Conservation of mass and/or energy can mostly hold automatically without additional computational efforts.[36,37] Models specifically for thermal and electrical transport behaviors based on the LBM have been developed.[22,23,38,39] Very recently the LBM has been used to predict effective thermal conductivities of multiphase microporous media by varying the local relaxation time.[24–26] Here we develop our previous model[24] further so as to predict the effective conductivities of FGMs.

To solve the partial differential equation (1) in a three-dimensional multiphase system, the evolution equation can be generally given as

$$g_\alpha(\mathbf{r}+\mathbf{e}_\alpha\delta_t,t+\delta_t)-g_\alpha(\mathbf{r},t)=-\frac{1}{\tau_n}[g_\alpha(\mathbf{r},t)-g_\alpha^{\text{eq}}(\mathbf{r},t)], \tag{5}$$

where g_α^{eq} is the local equilibrium distribution in each direction, $\mathbf{e}_\alpha$ the discrete lattice velocity, and τ_n the dimensionless relaxation time for local phase. For a three-dimensional 15-speed (D3Q15) model as shown in Fig. 2, there are

$$g_\alpha^{\text{eq}}=\begin{cases}0, & \alpha=0\\ \phi/9, & \alpha=1-6\\ \phi/24, & \alpha=7-14,\end{cases} \tag{6}$$

$$\mathbf{e}_\alpha = \begin{cases} (0,0,0), & \alpha = 0 \\ (\pm 1,0,0)c, (0,\pm 1,0)c, (0,0,\pm 1)c, & \alpha = 1-6 \\ (\pm 1,\pm 1,\pm 1)c & \alpha = 7-14, \end{cases} \tag{7}$$

and

$$\tau_n = \frac{9}{5}\frac{\lambda_n}{c^2 \delta_t} + 0.5, \tag{8}$$

where δ_t is the time step, and c a pseudosound speed whose value in theory can take any positive value provided the resulting τ_n value is within (0.5, 2).[22,31] Both the potential and flux can then be calculated according to[40]

$$\phi = \sum_\alpha g_\alpha, \tag{9}$$

$$q = \left(\sum_\alpha \mathbf{e}_\alpha g_\alpha\right)\frac{\tau_n - 0.5}{\tau_n}. \tag{10}$$

After the potential field is solved, the effective conductivity, λ_{eff}, can be determined,

$$\lambda_{\text{eff}} = \frac{L \cdot \int q \cdot dA}{\Delta\phi \int dA}. \tag{11}$$

For the Dirichlet boundary treatment, we follow the bounce-back rule of nonequilibrium distribution proposed by Zou and He,[41]

$$g_\alpha - g_\alpha^{\text{eq}} = -(g_\beta - g_\beta^{\text{eq}}), \tag{12}$$

where α and β represent the opposite directions, and the equilibrium distribution can be calculated based on the local boundary temperature. For the insulated boundaries, a specular reflection treatment is implemented to prevent heat flux from leaking along the insulate surfaces.[24] It has been proved that the current boundary treatments have the second order accuracies.[41]

III. RESULTS AND DISCUSSION

The present lattice Boltzmann method is now used to solve the governing equations of transport for the distribution of the potential ϕ and the effective conductivity λ_{eff} in a functionally graded material.

A. Benchmarks

To validate the algorithm and the code, our numerical predictions are compared with the theoretical solutions for three cube problems with given property gradations only along the z axis. Assume the property is position dependent only. Let the potential at the top surface maintain at ϕ_T and that at the bottom surface $\phi_B = 0$. The conductivity at the bottom surface is λ_0. We then define three different material gradations, the quadratic, the exponential, and the trigonometric, respectively, as used in Ref. 21:

$$\text{Quadratic:} \quad \lambda = \lambda_0(1+\beta z)^2, \tag{13}$$

$$\text{Exponential:} \quad \lambda = \lambda_0 e^{2\beta z}, \tag{14}$$

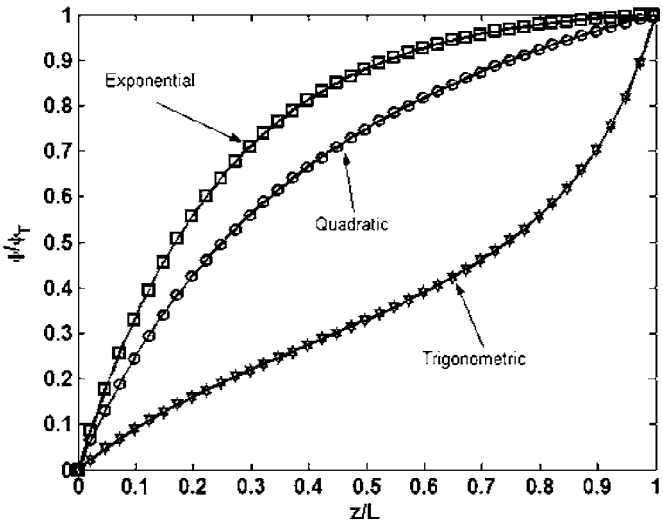

FIG. 3. Potential profiles in the z direction. The parameters used are $\lambda_0 = 10$, $\beta = 2$, $\phi_T = 1$, $L = 1$, and $a_1 = a_2 = 1$. The solid lines are analytical solutions and the symbols are numerical predictions.

$$\text{Trigonometric:} \quad \lambda = \lambda_0(a_1 \cos \beta z + a_2 \sin \beta z)^2. \tag{15}$$

The corresponding steady analytical solutions of the potential distribution for these three cases are

$$\text{Quadratic:} \quad \phi = \frac{\sqrt{\lambda_0}(1+\beta L) z \phi_T}{\sqrt{\lambda} L}, \tag{16}$$

$$\text{Exponential:} \quad \phi = \phi_T \frac{1 - e^{-2\beta z}}{1 - e^{-2\beta L}}, \tag{17}$$

$$\text{Trigonometric:} \quad \phi = \frac{\sqrt{\lambda_0}(a_1 \cos \beta L + a_2 \sin \beta L)\phi_T \sin \beta z}{\sqrt{\lambda} \sin \beta L}. \tag{18}$$

Figure 3 compares the potential distributions of the three analytical solutions with the numerical predictions using the present lattice Boltzmann method. The dimensionless parameters used are $\lambda_0 = 10$, $\beta = 2$, $\phi_T = 1$, $L = 1$, and $a_1 = a_2 = 1$. The solid lines are analytical solutions and the symbols are our numerical predictions. $200 \times 200 \times 200$ three-dimensional (3D) grids are used in the simulations. The results show excellent agreements, and thus validate initially the present algorithm and codes for predictions of effective conductivity of FGMs.

B. Actual functionally graded materials

Figure 4 shows a typical cross section of a FGM.[8] The real FGMs are often made of a series of layers with different component contents, and thus are discontinuous. Each component content increases or decreases monotonically across layers. Within each layer, the phase distributions are discrete as well. Similar to the microstructures of a granular porous medium, the phase distribution in each layer consists of one phase dispersed into another phase with random size, shape, position, and connections. Despite the heterogeneity, each layer has its own common effective conductivity.

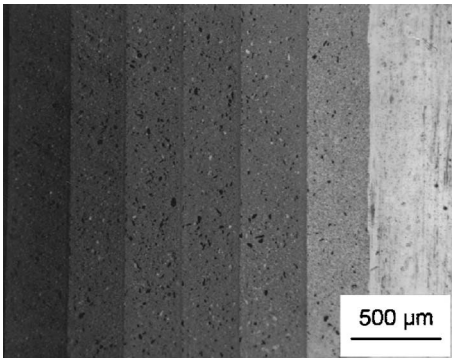

FIG. 4. A typical cross section of a real graded material.

To bring the major characteristics of a real FGM into our algorithm, the random effect has to be introduced during the reproduction of the morphology of the system. Although the random location of obstacles is the most simple and popular method to construct an artificial material,[17,42–44] it loses the details of shapes and connections of the dispersed phase. Recently, we have developed a random generation-growth algorithm for reproducing the microstructures of various granular porous media with random distribution and multiphase interactions.[24] In this study, we use this algorithm termed as quartet structure generation set (QSGS) to reproduce the multiphase distribution in each layer of the FGM. Figure 5 demonstrates the generated two-dimensional random phase distributions in a two-phase case (a), and a three-phase case (b), respectively, for one layer of the FGM using the QSGS method. In Fig. 5(a), the white portion is the dispersed (growing) phase and the dark the continuous matrix phase; while in Fig. 5(b) the gray is the first dispersed (growing) phase, the white the second dispersed (growing) phase, and the dark the continuous phase. The parameters used in the QSGS are $c_d=0.01$ P^2, $D_{1-4}:D_{5-8}=4$, $P^2=0.5$, $P^3=0.4$, and $I_i^{3,3}:I_i^{2,3}=1$ as explained in Ref. 24. Unless specified otherwise, we employ the same set of parameters for QSGS processes in all cases in this paper, and also use two-dimensional structures for easy illustration but three-dimensional ones for actual simulations.

Random features are clearly shown in the generated phase distributions, and the phase connections and interactions are included as well. Very similar structures have been observed in experiments for Al_2O_3/Y-TZP FGMs (two-phase case)[8] and ZrO_2/NiCoCrAlY FGMs (three-phase case).[45,46]

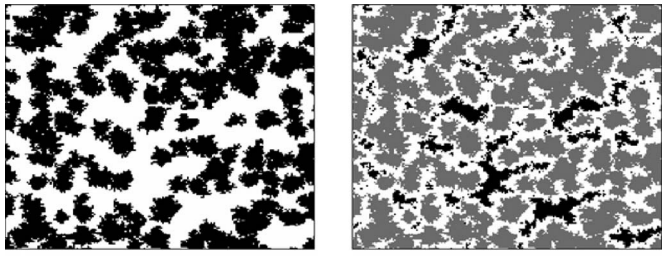

FIG. 5. Generated two-dimensional (2D) random phase distributions using QSGS for one layer of a real FGM. (a) Two-phase case; (b) three-phase case.

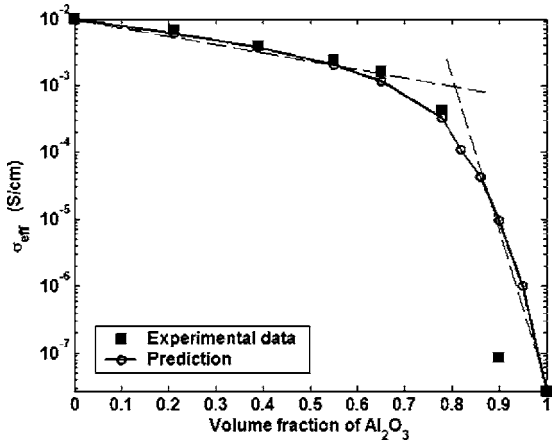

FIG. 6. Effective electric conductivity variation with volume fraction of Al_2O_3 for the uniform Al_2O_3/Y-TZP composites.

Once the random phase distributions for the FGM layers are produced, we then use our LBM approach to solve the transport governing equations for the multiphase material systems. The predicted results are finally compared with the available experimental data for both two-phase and three-phase cases.

For the two-phase case, we compare our predicted effective electric conductivities of the Al_2O_3/Y-TZP composite materials with the measurements by Sanchez-Herencia *et al.*[8] Figure 6 shows the results of effective electric conductivity versus volume fraction of Al_2O_3 for single-layer composites. The electric conductivities of the Al_2O_3 and Y-TZP components used in the simulations are 3.7×10^{-7} and 1.0×10^{-2} S/cm, respectively.[8] When we use a logarithmic scale for the y axis, the effective electric conductivity appears a nearly bilinear trend with the intersecting point falling around the point where the volume fraction of Al_2O_3 is 0.8. Before the intersecting point, the effective electric conductivity decreases with the volume fraction of Al_2O_3 at a low rate, whereas after the point, the decreasing rate becomes much steeper. Such a trend is consistent with the previous report.[8] Different from the previous predictions,[17] however, the change of the effective conductivity is smooth and continuous with no singular point, making more sense in physics. Our predictions agree well also with the experimental data when the Al_2O_3 volume fraction is below 0.8, yet the predicted electric conductivity is much greater than the measured value once the Al_2O_3 volume fraction approaches 0.9. The reason for the discrepancy, as pointed in Ref. 17, might lie in the systematic error of the experimental equipment or the lacuna existing in the materials. Next, we calculated the effective properties of multilayer FGMs with parameters reported in the experiments.[8] The predicted effective electric conductivities, against the average volume fraction of Al_2O_3, are compared with the experimental data in Fig. 7. Once again good agreements are obtained.

For a three-phase case, we consider the effective thermal conductivity in a ZrO_2/NiCoCrAlY system as dealt with by Khor and Gu in Ref. 45. This ZrO_2/NiCoCrAlY FGM is actually a three-phase system, for the porosity (air volume fraction) in the material increases with the fraction of ZrO_2

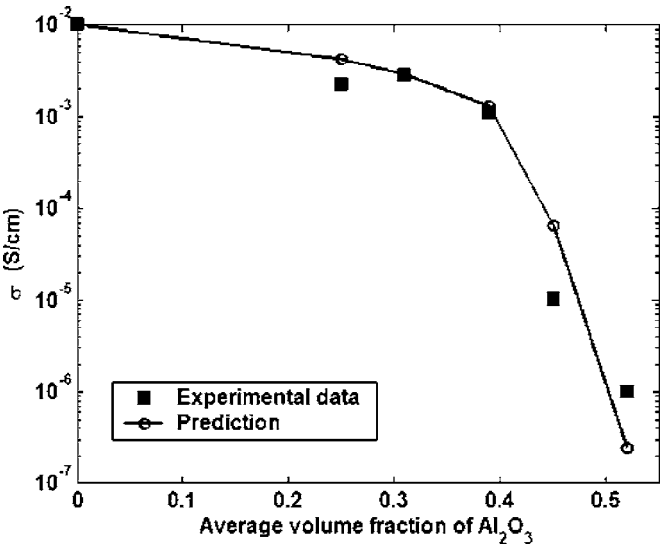

FIG. 7. Effective electric conductivity variation with average volume fraction of Al_2O_3 for the Al_2O_3/Y-TZP FGMs.

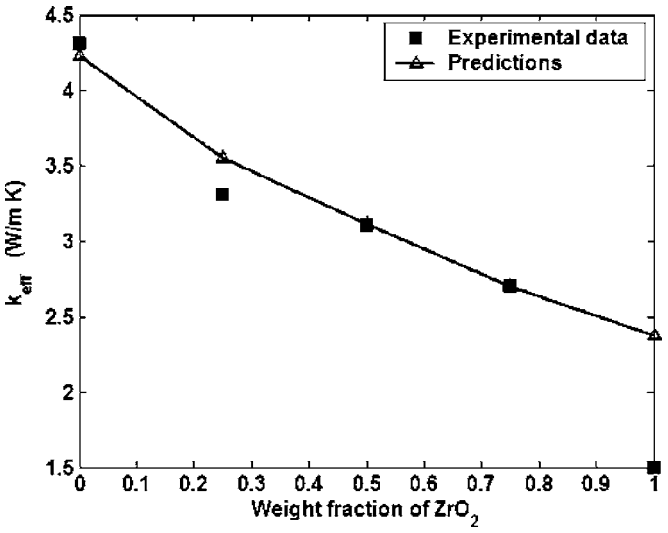

FIG. 8. Effective thermal conductivity variation with weight fraction of ZrO_2 for the ZrO_2/NiCoCrAlY FGMs.

up to 12.16%. The air has a much lower thermal conductivity than the other materials in the system so that it would be a gross negligence if the contribution from the entrapped air is excluded from calculation. However, no attempts have been taken to account for the influence of the entrapped air. In this work, we reproduce this three-phase structure, ZrO_2/NiCoCrAlY/air, using the QSGS method and then calculate the effective thermal conductivities. The phase fraction parameters are listed in Table I where the following relation is used to determine the volume fraction for a give weight fraction:

$$V_f = \frac{W_f}{W_f + (1 - W_f)\rho_2/\rho_1}, \tag{19}$$

where V_f is the volume fraction, W_f the weight fraction, ρ_2 the density of the dispersed phase, and ρ_1 the density of the matrix phase. Figure 8 shows the predicted effective thermal conductivities of a ZrO_2/NiCoCrAlY FGM compared with the experimental data measured by Khor and Gu.[45] Both the thermal conductivity and density used in our simulations are 3 W/m K and 6 g/cm^3 for pure ZrO_2, and 5 W/m K and 7.324 g/cm^3 for pure NiCoCrAlY, respectively. The thermal conductivity of air is 0.025 W/m K in the simulations.[24] For ZrO_2-only porous materials, big cracks have been reported due to the difficulty in remelting ZrO_2 powders during spraying.[45] As a result, the measured thermal conductivity is much lower than the predicted one. Otherwise, the present predictions are consistent with the experimental data.

TABLE I. Phase fraction parameters for the ZrO_2/NiCoCrAlY FGMs.

ZrO_2 (wt %)	NiCoCrAlY (wt %)	Porosity (vol %)	ZrO_2 (vol %)	NiCoCrAlY (vol %)
0	100	7.5	0	92.5
25	75	8.9	26.34	64.76
50	50	9.9	49.51	40.59
75	25	11.1	69.82	19.08
100	0	12.16	87.84	0

C. Predictions of other properties

Our present methodology can be extended to predict a couple of other effective properties of multiphase FGMs, due to their similarities in physics or in governing equations. For instance, of dielectric permittivity of porous glass with different fillers reported by Sen *et al.*[47] We have noticed that the measurement technique used by them was based on the two-electrode method and it is equivalent to the hot probe technique found in thermal conductivity measurement. Early work has proved that such axis-symmetrical techniques are essentially two-dimensional techniques[48] so that the experimental data thus obtained are comparable to two-dimensional predictions. We performed a two-dimensional QSGS process to regenerate the structure, and solved the corresponding governing equations by a D2Q9 LBM.[24] The calculated dielectric permittivities are then compared in Fig. 9 with the experimental data of Sen *et al.* The component

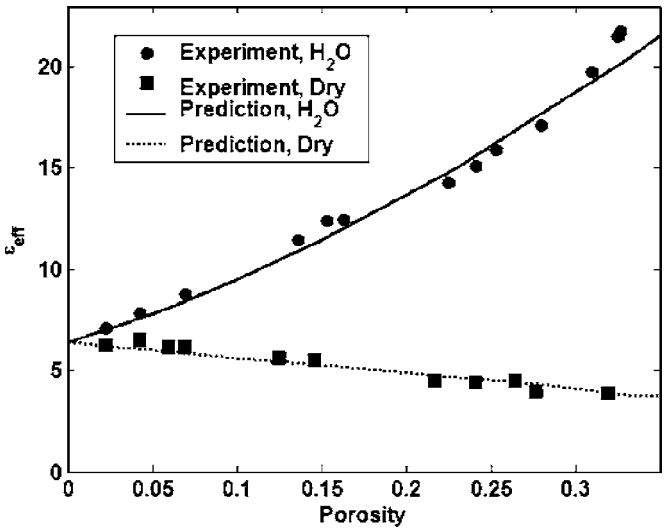

FIG. 9. Effective dielectric permittivity vs porosity for porous glass filled with different fillers.

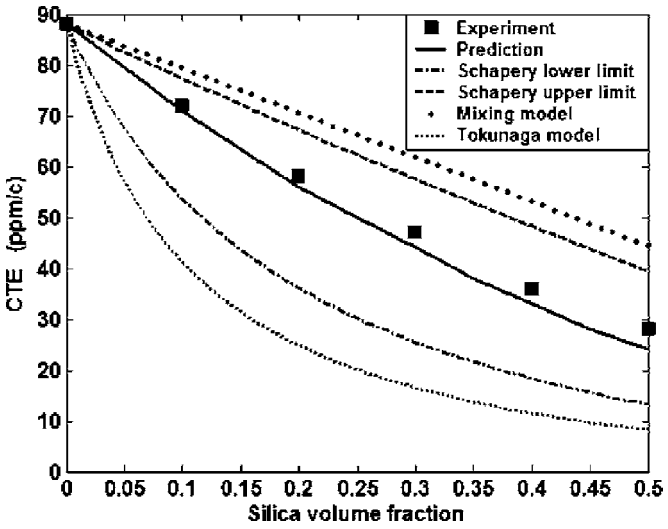

FIG. 10. Coefficient of thermal expansion of epoxy resin/silica composites.

properties used are $\varepsilon_r^{\text{water}}=80$, $\varepsilon_r^{\text{air}}=1$, and $\varepsilon_r^{\text{glass}}=6.4$ from Ref. 47. Once again, very good consistence exists between the two.

Generally speaking, the mechanical properties are governed by different physics from that for transport phenomena. However, it is reported that some effective mechanical properties of two-phase composites, such as the elastic modulus and coefficient of thermal expansion, obey the similar combination laws as the effective conductivities do.[49] In this contribution, we attempted to predict the effective coefficient of thermal expansion of some epoxy resin/silica composites by using our present approach. Figure 10 compares the predicted effective coefficients of thermal expansion (CTE) with the experimental data, as well as the predictions by other theoretical models.[49] The component coefficients of the thermal expansion used in simulations are 88.0 and 0.5 ppm/K for epoxy resin and silica, respectively,[49] and our predictions in Fig. 10 agree much better with the experimental data than other theoretical predictions.

IV. CONCLUSIONS

This paper presents a numerical approach for prediction of the effective conductivities for multiphase FGMs with random phase distribution and multiphase interactions. Firstly, the multiphase microstructures of the FGMs are reproduced by a random generation-growth algorithm, and then the corresponding transport governing equations are solved by a high-efficiency lattice Boltzmann method. The effective electric and thermal conductivities thus predicted agree well with the published experimental data for both two- and three-phase FGMs. The methodology has also been extended to other transport and physical properties of multiphase composites such as dielectric permittivity and thermal expansion coefficients, validated again by available experimental data. All the cases provided here exhibit the predictive power and the wide applicability of the methods developed in this paper.

ACKNOWLEDGMENT

The present work is supported by the grants from the NTC-M04-CD01 and NBRPC-2007CB206901.

[1] Y. Miyamoto, W. A. Kaysser, B. H. Rabin, A. Kawasaki, and R. G. Ford, *Functionally Graded Materials: Design, Processing, and Applications* (Kluwer, Boston, MA 1999).
[2] G. H. Paulino, Z. H. Jin, and R. H. Dodds, Jr., in *Comprehensive Structural Integrity*, edited by B. Karihaloo and W. G. Knauss (Elsevier Science, Amsterdam, 2003), Vol. 2, pp. 607–644.
[3] M. Ivosevic, R. Knight, S. R. Kalidindi, G. R. Palmese, and J. K. Sutter, *Microstructure and Properties of Thermally Sprayed Functionally Graded Coatings for Polymeric Substrates Cleveland, Ohio* (NASA Glenn Research Center, Cleveland, OH, 2003).
[4] N. Araki, D. W. Tang, and A. Ohtani, Int. J. Thermophys. **27**, 209 (2006).
[5] A. H. Wu, W. B. Cao, C. C. Ge, J. F. Li, and A. Kawasaki, Mater. Chem. Phys. **91**, 545 (2005).
[6] E. M. Carrillo-Heian, R. Douglas Carpenter, G. H. Paulino, J. C. Gibeling, and Z. A. Munir, J. Am. Ceram. Soc. **84**, 962 (2001).
[7] X. Zhu, Q. Wang, and Z. Meng, J. Mater. Sci. Lett. **14**, 516 (1995).
[8] A. J. Sanchez-Herencia, R. Moreno, and J. R. Jurado, J. Eur. Ceram. Soc. **20**, 1611 (2000).
[9] K. Eguchi, T. Hoshino, and T. Fujihara, in *Third International Symposium on Structural Functional Gradient Materials, Proceedings of FGM '94*, edited by B. Ilschner and N. Cherradi (Polytechnic University Romandes Press, Lausanne, Switzerland, 1995), pp. 619–625.
[10] M. Niino and M. Koizumi, in *Third International Symposium on Structural and Functional Gradient Materials, Proceedings of FGM '94*, edited by B. Ilschner and N. Cherradi (Polytechnic University Romandes Press, Lausanne, Switzerland, 1995), pp. 601–605.
[11] S. Suresh and A. Mortensen, *Fundamentals of Functionally Graded Materials: Processing and Thermomechanical Behaviour of Graded Metals and Metal-Ceramic Composites* (IOM Communications, London, 1998).
[12] A. Mortensen and S. Suresh, Int. Mater. Rev. **40**, 239 (1995).
[13] G. H. Paulino, Eng. Fract. Mech. **69**, 1519 (2002).
[14] H. M. Yin, G. H. Paulino, W. G. Buttlar, and L. Z. Sun, J. Mech. Phys. Solids **55**, 132 (2007).
[15] J. N. Reddy and C. D. Chin, J. Therm. Stresses **21**, 593 (1998).
[16] J. Aboudi, M. J. Pindera, and S. M. Arnold, Composites, Part B **30**, 777 (1999).
[17] H. M. Yin, G. H. Paulino, W. G. Buttlar, and L. Z. Sun, J. Appl. Phys. **98**, 063704 (2005).
[18] J. R. Cho and D. Y. I. Ha, Comput. Methods Appl. Mech. Eng. **191**, 3195 (2002).
[19] B. L. Wang and Z. H. Tian, Finite Elem. Anal. Design **41**, 335 (2005).
[20] J. H. Kim and G. H. Paulino, Int. J. Numer. Methods Eng. **53**, 1903 (2002).
[21] A. Sutradhar and G. H. Paulino, Comput. Methods Appl. Mech. Eng. **193**, 4511 (2004).
[22] J. K. Wang, M. Wang, and Z. X. Li, Int. J. Therm. Sci. **46**, 228 (2007).
[23] J. K. Wang, M. Wang, and Z. X. Li, Commun. Nonlinear Sci. Numer. Simul. (in press).
[24] M. Wang, J. K. Wang, N. Pan, and S. Y. Chen, Phys. Rev. E **75**, 036702 (2007).
[25] M. Wang, J. H. He, J. Y. Yu, and N. Pan, Int. J. Therm. Sci. **46**, 848 (2007).
[26] M. Wang, N. Pan, J. K. Wang, and S. Y. Chen, J. Colloid Interface Sci. **311**, 562 (2007).
[27] X. Chen and P. Han, Int. J. Heat Fluid Flow **21**, 463 (2000).
[28] E. Tuncer and S. M. Gubanski, J. Appl. Phys. **89**, 8092 (2001).
[29] S. Y. Chen and G. D. Doolen, Annu. Rev. Fluid Mech. **30**, 329 (1998).
[30] D. Raabe, Modell. Simul. Mater. Sci. Eng. **12**, R13 (2004).
[31] J. K. Wang, M. Wang, and Z. X. Li, J. Colloid Interface Sci. **296**, 729 (2006).
[32] Q. J. Kang, D. X. Zhang, and S. Y. Chen, J. Geophys. Res. **108**, 2505 (2003).
[33] Q. J. Kang, D. X. Zhang, P. C. Lichtner, and I. N. Tsimpanogiannis, Geophys. Res. Lett. **31**, L21604 (2004).
[34] M. Wang, J. K. Wang, S. Y. Chen, and N. Pan, J. Colloid Interface Sci. **304**, 246 (2006).
[35] M. Wang, J. K. Wang, N. Pan, and S. Y. Chen, Commun. Comput. Phys. **2**, 1055 (2007).
[36] G. D. Doolen, *Lattice Gas Methods for Partial Differential Equations*

(Addison-Wesley Longman, New York, 1990).
[37]S. Succi, *The Lattice Boltzmann Equation for Fluid Dynamics and Beyond* (Oxford Science, London, 2001).
[38]X. Y. He, S. Y. Chen, and G. D. Doolen, J. Comput. Phys. **146**, 282 (1998).
[39]Y. Peng, C. Shu, and Y. T. Chew, Phys. Rev. E **68**, 026701 (2003).
[40]A. D'Orazio and S. Succi, Lect. Notes Comput. Sci. **2657**, 977 (2003).
[41]Q. S. Zou and X. Y. He, Phys. Fluids **9**, 1591 (1997).
[42]Y. Shoshany, D. Prialnik, and M. Podolak, Icarus **157**, 219 (2002).
[43]S. Barta and P. Dieska, Kovove Mater. **40**, 99 (2002).
[44]H. F. Zhang, X. S. Ge, and H. Ye, J. Phys. D **39**, 220 (2006).
[45]K. A. Khor and Y. W. Gu, Thin Solid Films **372**, 104 (2000).
[46]K. A. Khor, Y. W. Gu, and Z. L. Dong, Surf. Coat. Technol. **139**, 200 (2001).
[47]P. N. Sen, C. Scala, and M. H. Cohen, Geophysics **46**, 781 (1981).
[48]M. Wang, J. K. Wang, N. Pan, S. Y. Chen, and J. He, J. Phys. D **40**, 260 (2007).
[49]C. P. Wong and R. S. Bollampally, J. Appl. Polym. Sci. **74**, 3396 (1999).